Available online at www.sciencedirect.com
ScienceDirect
Journal of the Mechanics and Physics of Solids 56 (2008) 1203–1223
JOURNAL OF THE MECHANICS AND PHYSICS OF SOLIDS
www.elsevier.com/locate/jmps

# On the nonlocal nature of dislocation nucleation during nanoindentation

R.E. Miller[a,*], D. Rodney[b]

[a]*Department of Mechanical and Aerospace Engineering, Carleton University, 1125 Colonel By Drive, Ottawa, Ont., Canada K1S 5B6*
[b]*Science et Ingénierie des Matériaux et Procédés (UMR CNRS 5266), INP Grenoble, BP46, 38402 St. Martin D'Hères, France*

Received 27 July 2007; received in revised form 15 October 2007; accepted 17 October 2007

**Abstract**

Using static atomistic simulations, we study the full details of the mechanism by which dislocations homogeneously nucleate beneath the surface of a initially defect-free crystal during indentation. The mechanism involves the collective motion of a finite disk of atoms over two adjacent slip planes, the diameter of which depends on the indenter size. The nucleation mechanism highlights the need for *nonlocal* considerations in the development of a nucleation criterion. We review three nucleation criteria from the literature, each of which is based on purely *local* measures of the state of stress, and show that none are sufficiently general to predict nucleation in realistic atomic systems. We then propose a criterion based on an eigenmode analysis of the atomic-scale acoustic tensor. We demonstrate the accuracy of the criterion, which also works in the presence of existing topological defects like free surfaces or dislocation cores. The dependence of the size of the nucleated disk on the indenter radius leads to a self-similar nucleation process and virtually no indentation size effect (ISE), suggesting that homogeneous nucleation is only possible for very small indenters.


*Keywords:* Dislocation nucleation; Nanoindentation; Atomistic modeling; Nucleation criterion; Indentation size effects

## 1. Introduction

This work poses a fundamental question: What are the mechanical conditions inside a crystalline solid that give rise to the nucleation of a dislocation? And further, can we analyze a crystal in some deformed state and predict, *a priori*, where a new dislocation will form. In other words, we are looking for a general criterion for dislocation nucleation.

Dislocation nucleation, both homogeneous nucleation and heterogeneous nucleation at defects such as surface steps, vacancies and grain boundaries, has been studied by many authors (Kelchner et al., 1998; Miller et al., 2003; Li et al., 2002; van Vliet et al., 2003; de la Fuente et al., 2002; Lilleodden et al., 2001; Lilleoden et al., 2003; Knap and Ortiz, 2003; Tadmor et al., 1999; Christopher et al., 2001; Shenoy et al., 2000; Zimmerman et al., 2001a,b; Zhu et al., 2004; Li et al., 2004). Although it is usually clear when and

*Corresponding author.
*E-mail addresses:* rmiller@mae.carleton.ca (R.E. Miller), drodney@gpm2.inpg.fr (D. Rodney).

0022-5096/$ - see front matter © 2007 Elsevier Ltd. All rights reserved.
doi:10.1016/j.jmps.2007.10.005

where defects form, the pathway through configuration space (taking the crystal from defect-free and stressed to defected and less-stressed) has never been analyzed in detail. Our aim is to formulate a nucleation criterion, and as such we need to understand the full details of the behavior of the crystal at the point of instability.

Our simulations are similar to many that have been cited above. We perform quasistatic, zero temperature atomistic simulations of an ideal spherical indenter and an initially defect-free crystal. We consider both 2D and 3D crystals, modeled using the Ercolessi and Adams (1994) interatomic potentials for aluminum. The 2D crystals are a model triangular lattice and the 3D crystals are face-centered cubic (fcc).

This is not the first work to propose a dislocation nucleation criterion. Later, we examine three existing alternatives. (1) We look at how one can extend the model of Rice (Rice, 1992; Sun et al., 1993; Rice and Beltz, 1994) (originally proposed for nucleation from a crack tip) to homogeneous nucleation, (2) we re-visit a version of the Hill criterion for material instability (Hill, 1962) extended down to the atomic scale by Li et al. (2002) and van Vliet et al. (2003), and (3) we examine the stress-gradient-based criterion of Miller and Acharya (2004). We argue that none of these three criteria are sufficiently general to capture homogeneous nucleation, in particular because they are all based on *local* measures of the state of deformation or stress. As we will show, the nucleation mechanism is inherently *nonlocal*.

We propose a new criterion inspired by the atomic-scale Hill approach (van Vliet et al., 2003), and related to phonon stability methods (Born and Huang, 1954; Li et al., 2004; Dobson et al., 2007) and failure theories derived from the acoustic tensor (Steinmann et al., 2007). In essence, the eigenmode analysis of a small group of atoms around each point in space reveals when a zero-energy eigenmode corresponding to dislocation nucleation emerges in the acoustic tensor. We show that the criterion is highly accurate in both 2D and 3D indentation simulations. It has the further advantage over existing criteria that it remains accurate near existing topological defects (for example, a free surface or a pre-existing dislocation core).

There are many experimental observations of the initial stages of plasticity during nanoindentation, shedding light on our understanding of the load levels and mechanisms of dislocation nucleation (Gerberich et al., 1996; Corcoran et al., 1997; Suresh et al., 1999; Chiu and Ngan, 2002). The question of whether homogeneous nucleation can even be observed experimentally has recently been put forth by Schuh et al. (2005) and Mason et al. (2006), whose experiments suggest that the energy barriers for homogeneous nucleation may be too large to explain the statistics of pop-in events during indentation. As such, they propose that nucleation is likely to be aided by the presence of vacancies in the crystal and therefore is not truly homogeneous. Here, we make at least one observation in support of that idea: we find that homogeneous nucleation mechanism involves larger and larger numbers of atoms as the indenter size grows. For large indenters, the chance of finding a sufficiently large region that is free of vacancies or other defects is quite small, and homogeneous nucleation seems, therefore, unlikely.

The outline of the remainder of the paper is as follows. In Section 2 we present the results of our indentation simulations, first in 2D and then in 3D. Section 3 reviews the three existing criteria from the literature and provides insights into why they are not sufficient. We then present our new criterion in Section 4 and show its successful predictions in both 2D and 3D, after which we conclude with a brief summary and suggestions for future work.

## 2. Dislocation nucleation simulations

We press a rigid, frictionless sphere into an initially perfect single crystal at zero Kelvin and watch the initial nucleation of a dislocation. In 2D, we will use a simple triangular lattice of atoms, interacting with the Ercolessi–Adams (1994) EAM potentials. The 2D lattice has a near-neighbor distance of $a_0 = 2.83\,\text{Å}$. We will use the same Al potentials to look at fcc crystals ($a_0 = 4.032\,\text{Å}$). The frictionless indenter is modeled as a repulsive potential of the form

$$\Phi(r) = \begin{cases} A(R-r)^2 & \text{if } r \leqslant R, \\ 0 & \text{if } r > R, \end{cases} \tag{1}$$

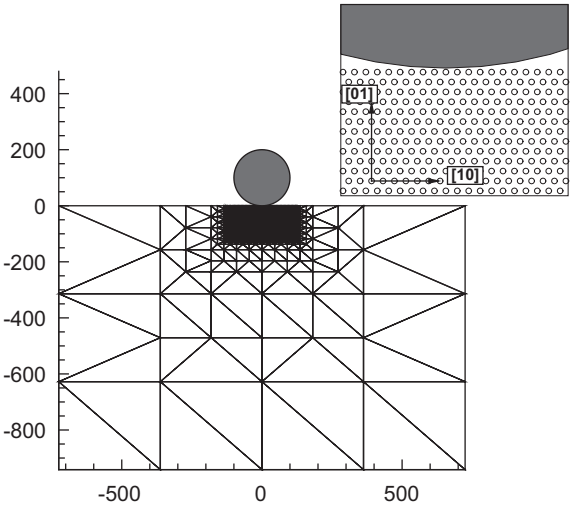


Fig. 1. Indentation into a 2D triangular lattice along the [0 1] direction.

where $A = 1\,\mathrm{eV/\AA^2}$ is chosen as the strength of the interaction. $R$ is the indenter radius, chosen here to be $R = 100\,\mathrm{\AA}$ unless otherwise specified. Several previous authors have used similar indenter potentials (Kelchner et al., 1998; Knap and Ortiz, 2001; Li et al., 2002; Miller et al., 2003; Miller and Acharya, 2004).

### 2.1. 2D results

As a representative example of the 2D case, we discuss results for indentation along the [0 1] direction in the 2D lattice as shown in Fig. 1. We use the static quasicontinuum (QC) simulation method (Shenoy et al., 1999; Tadmor and Miller, 2007). The region beneath the indenter, extending approximately from $-130$ to $130\,\mathrm{\AA}$ horizontally and from $-120$ to $0\,\mathrm{\AA}$ vertically is fully atomistic, and the inset on the top right shows the details of the lattice beneath the indenter.[1] Initial contact between the indenter and the crystal occurs at the origin ($\{x, y\} = \{0, 0\}$).

Load steps are taken by uniformly compressing the entire model along the vertical direction, such that the atom that is closest to the indentation axis and in contact with the indenter moves an amount $\Delta d$, the same amount as the increment of indenter displacement. The bottom row of finite element (FE) nodes and the indenter are then held fixed and the rest of the model is allowed to relax by conjugate gradient (CG) energy minimization. Each subsequent load step uses the relaxed configuration from the previous step as a starting point and the process repeats. The uniform compression of the model permits larger load steps to be taken than if we just moved the indenter into the crystal: $20\,\mathrm{\AA}$ compared to typically $1\,\mathrm{\AA}$ or less.

Because our interest is in the first nucleation of a defect and the equilibrium atomistic configuration *just prior to this event*, we want to take very small load steps as we approach the critical indenter penetration. To do this, an algorithm was used whereby a given load step, $\Delta d$, is chosen and repeated until a defect nucleates. At this point, the last relaxed configuration *prior to* nucleation is restored, the size of the load step is reduced by a factor of 2, and the process repeated until the load step size is below some tolerance. In this way, we have been able to capture the configuration of the atoms so close to nucleation that subsequent indenter motion of less than $1 \times 10^{-6}\,\mathrm{\AA}$ triggers nucleation, implying that the final elastic configuration is, for all practical purposes, *right at* the point of instability leading to the first defect nucleation.

The load–displacement curve for this indentation is shown in Fig. 2. The points are the actual load steps taken, which are initially large and then adaptively get smaller and smaller as previously discussed. The inset shows the final, tiny load steps and the load drop at nucleation. In Fig. 3, we see the region under the indenter

[1]The use of the QC method is limited, in this case, to providing a large hyperelastic foundation in which a smaller atomistic simulation is embedded. It serves only to allow more realistic boundary conditions with fewer atomic degrees of freedom.

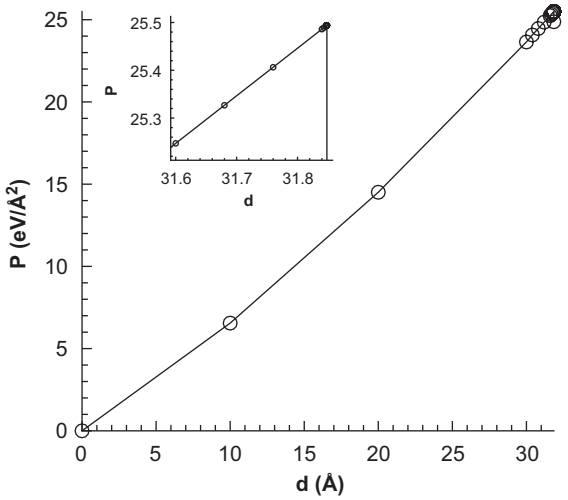


Fig. 2. Load–displacement curve for indentation into a 2D triangular lattice along the [0 1] direction.

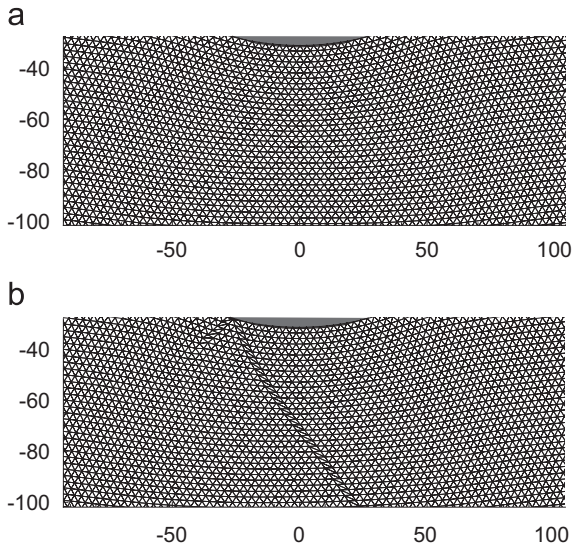


Fig. 3. Configurations: (a) just before and (b) just after dislocation nucleation during indentation into a 2D triangular lattice along the [0 1] direction.

just before and just after nucleation. A mesh is shown between the atoms, rather than the atoms themselves, to better appreciate the plastic deformation. The sheared elements indicate the plane along which slip has taken place, leaving a dislocation near the surface at the left edge of the indenter and another out of view towards the lower right side. The unstable nature of the nucleation process, coupled with the low Peierls barrier, means that the dislocations travel a long way from their initial nucleation site. To see the details of the nucleation itself and its exact location, it is necessary to look at intermediate configurations *during* the CG minimization between relaxed configurations (a) and (b) in Fig. 3, i.e., at each configuration after a line minimization step.[2]

Fig. 4 reveals the exact moment of dislocation nucleation by comparing the CG minimization steps just before and after the defect forms. We can see that the nucleation event is the instantaneous appearance of a

[2]We have repeated this approach using different energy minimizing techniques, specifically a steepest descent algorithm and a "Verlet" quenched-dynamics algorithm to verify that the mechanism is independent of the details of the minimization technique.

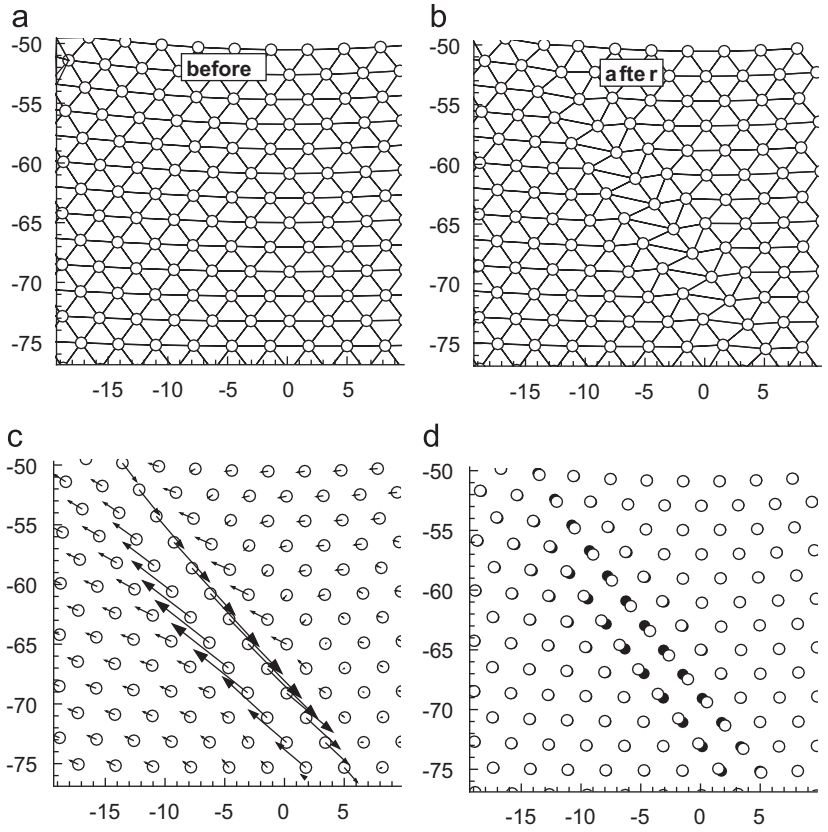


Fig. 4. Conjugate gradient minimization steps: (a) just before and (b) just after nucleation. Vectors in (c) show the displacements of each atom during the minimization step magnified by a factor of 10, while (d) superimposes the atomic positions from (a) (shown in black) beneath those from (b) (shown in white).

dislocation dipole of finite size, corresponding to the collective motion of about 10 atoms on either side of the slip plane. One row of 10 atoms moves about 0.6 Å along the slip direction, while the next row moves about the same distance in the other direction. Other than these 20 or so atoms, there is very little movement. The value of 0.6 Å corresponds to about $\frac{1}{4}$ of the Burgers vector, so that the total slip in the region is about $b/2$. After the formation of this "nucleus", the formation of the full defect proceeds in two more steps. First, the Burgers vector of the dipole grows to reach the full $b$. Within about 10 minimization steps, the dislocation is fully formed and the dipole spacing has grown only slightly, to about 13 atomic spacings. Only then does the final step take place, during which the fully formed dipole moves apart. However, although the final configuration involves two fully formed dislocations with a large separation between them, the true *nucleus* of plasticity is a dipole with about half the full Burgers vector.

This nucleation process is apparently a signature of the indentation simulations, regardless of the crystal orientation, indenter size or model dimensionality (although of course the load level and precise location of the initial defect change). The size of this dipole is more or less constant with respect to the orientation of the crystal, *but grows with the size of the indenter*, an interesting point that we will return to later. In 3D, this process becomes the spontaneous formation of a loop, again of a finite size depending only on the size of the indenter. We refer to the diameter of this critical nucleating disk (or dipole in 2D) as the "nucleation diameter", $d_{\mathrm{nuc}}$.

### 2.2. Effect of indenter size

We studied the dependence of the nucleation diameter $d_{\mathrm{nuc}}$ on the indenter radius $R$ by systematically varying $R$ from a minimum of 20 Å to a maximum of 200 Å for the 2D indentation along [0 1], keeping the

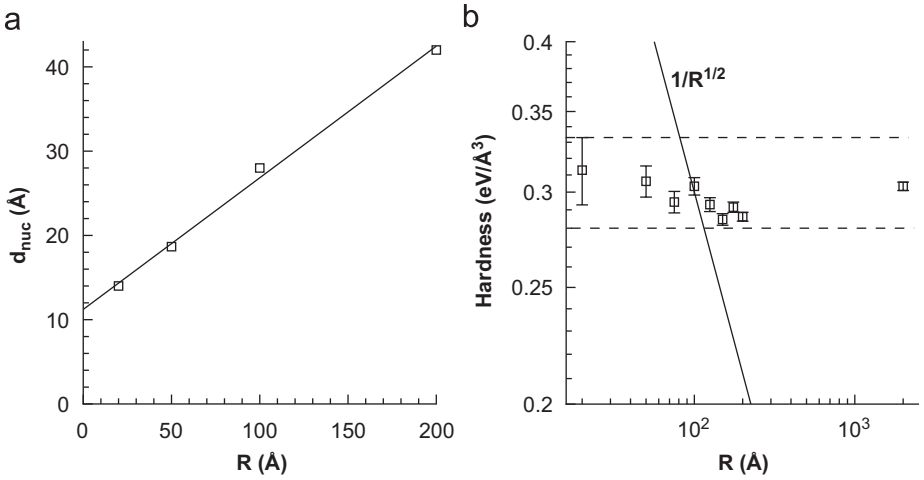


Fig. 5. (a) Effect of indenter size on the size of the nucleating disk, $d_{nuc}$. (b) Effect of indenter size on the critical load per unit contact area ("hardness"). Error bars represent the uncertainty in determining the contact area, which varies discontinuously as additional atoms contact the edges of the indenter, and the dashed lines in the figure bound all data points between values of $H = 0.280\,\mathrm{eV/\AA^3}$ and $H = 0.333\,\mathrm{eV/\AA^3}$.

model boundaries constant as shown in Fig. 1. An admittedly subjective estimate of $d_{nuc}$ for these cases, made by examining the nucleation processes by eye, is plotted in Fig. 5(a) to show an approximately linear dependence. In all cases, the mechanism is qualitatively identical to that shown in Fig. 4. The only difference is the size of the critical disk, $d_{nuc}$.

From these simulations, we can compute the "hardness" associated with the first nucleation event, which is defined as the force on the indenter divided by the contact area (contact length in 2D) just prior to nucleation. The results are plotted in Fig. 5(b). Additionally, we built one much larger model spanning approximately 20,000 Å in the horizontal direction and 11,000 Å vertically, with a 400 Å × 300 Å atomistic region embedded at the location where nucleation was expected to occur, and computed the hardness for an indenter radius of $R = 2000$ Å. We see a very weak size dependence within the points from $R = 20$ to 200 Å, certainly due to the fact that the fixed model boundaries are having some influence. By way of contrast, in the figure we compare this size dependence with a curve of the inverse square root form (which is the usual dependence of the experimentally well-known indentation size effect (ISE), (Nix and Gao, 1998; Gerberich et al., 2002). This curve emphasizes the extremely weak dependence found here. Other than a weak influence of the far-field boundary, we conclude that there is essentially no indenter-size dependence of the disk radius, $d_{nuc}$.

Note that since the critical disk grows with the indenter size, we expect that homogeneous nucleation would rapidly become highly unlikely as the indenter size increases. This is because the probability of such a large region of crystal being free of any defects (including vacancies) becomes very small. On the other hand, for very small indenters, homogeneous nucleation may in fact occur.

### 2.3. 3D results

The 3D fcc crystal was oriented so that indentation took place along one of the three different directions: [1 0 0], [1 1 0] and [1 1 1]. In each case, the simulation cell was roughly cubic with all edges exceeding 120 Å in length and each cell containing about 120,000 atoms. Periodic boundary conditions were used in the two directions normal to the direction of indentation. The indented surface was free and the opposite surface was held fixed. In the 3D simulations, we do not use the adaptive load-stepping algorithm described in Section 2.1. Instead, the indenter displacement step is constant at 0.25 Å.

In these simulations, defects form below the surface, via the homogeneous nucleation of glissile Shockley partial loops on {1 1 1} planes. Depending on the orientation of the crystal with respect to the indenter, these glissile loops form at different locations, reflecting the symmetries and plastic anisotropy of the crystal. In the

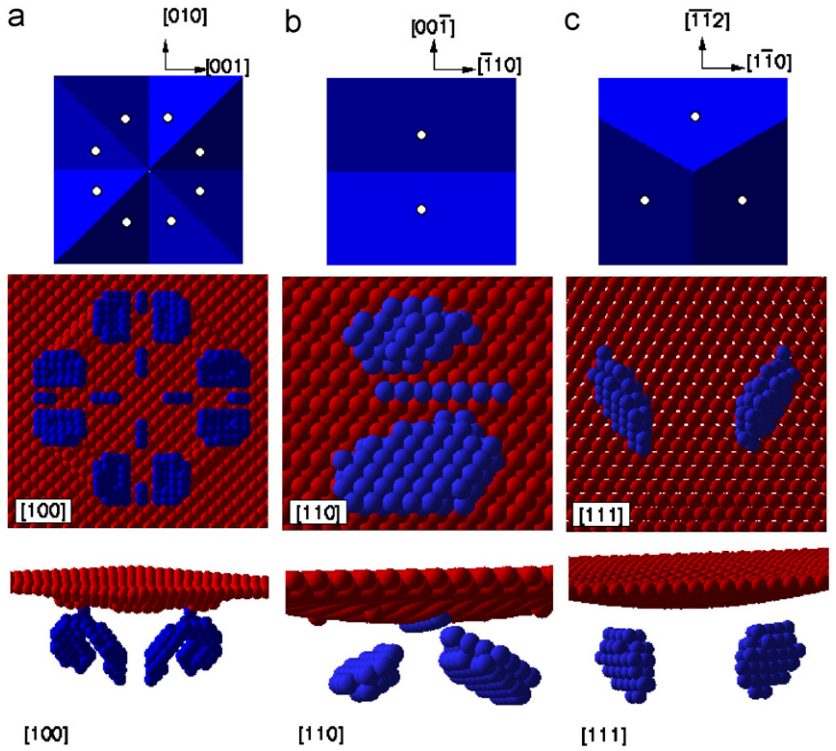


Fig. 6. Dislocation nucleation in 3D. The top row schematically shows nucleation sites beneath the indenter for indentation along (a) ⟨1 0 0⟩, (b) ⟨1 1 0⟩, and (c) ⟨1 1 1⟩. The center and bottom rows show actual nucleation events. The center row shows a view from the bottom, while the bottom row shows an alternate view to better reveal the structure. On the left, the simultaneous nucleation of eight loops on the active slip planes during indentation along ⟨1 0 0⟩. In the center, two loops form during indentation along ⟨1 1 0⟩. On the right, two of the three possible nucleation sites activate during indentation along ⟨1 1 1⟩.

top row of Fig. 6, we show schematically the symmetric locations where defects will nucleate under the indenter for the three indentation orientations considered here. In each image we show the view from inside the crystal, looking up towards the indenter (bottom view), of the relevant {1 1 1} planes, with a light source situated at the top left of each image to highlight the orientation of the planes. The exact nucleation location, in terms of the depth below the surface and the distance from the indenter's center will depend on the stiffness and strength of the crystal, the radius of the indenter, and the size of the model. Also, in actual simulations the loops do not always appear simultaneously due to numerical noise.

Qualitative snapshots of the nucleation process, painting the general picture of how and where the initial defects form, are abundant in the literature (Kelchner et al., 1998; van Vliet and Suresh, 2002; Knap and Ortiz, 2003; van Vliet et al., 2003; Li, 2007), and our results are consistent with those of others. Further, we find that the critical nucleation process is well-approximated by the 3D extension of our 2D observations. That is to say that there is a rigid sliding of atomic disks in two adjacent {1 1 1} planes, one over the other, in the direction of the Shockley partial Burgers vector. The disk size, $d_{\mathrm{nuc}}$, appears to be approximately constant between the three orientations.

In Fig. 6, we show images of intermediate configurations *during* a CG minimization, and atoms are shown only if they are near the free surface (red) or they have moved a relatively large amount during the CG step (blue). Typical atomic motions shown are on the order of 0.1 Å. It is important to note that these configurations would not show anything using the centrosymmetry parameter (Kelchner et al., 1998) or a first-neighbor analysis (Rodney, 2004) to highlight dislocations. These atoms are just in the process of moving to form a disk of slipped crystal. The leftmost images are about as early in the process as can be observed.

Table 1
Locations (relative to the initial point of indenter contact at (0, 0, 0)) and types of the nucleated defects in the 3D simulations

| Indent dir'n | Disl. location (Å) | Disl. type |
|---|---|---|
| [1 0 0] | (−19.32, −15.26, 8.35) | (1 1 1)[$\bar{1}$ $\bar{1}$ 2] |
| | (8.35, −15.27, −19.32) | (1 1 1)[$\bar{1}$ $\bar{1}$ 2] |
| | (21.22, −8.13, 6.47) | (1 $\bar{1}$ 1)[$\bar{1}$ 1 2] |
| | (−6.52, −10.1, −19.24) | (1 $\bar{1}$ 1)[$\bar{1}$ 1 2] |
| | (21.21, −8.13, −6.48) | (1 1 $\bar{1}$)[1 1 2] |
| | (−6.52, −10.1, 19.23) | (1 1 $\bar{1}$)[1 1 2] |
| | (−19.24, −10.1, −6.52) | ($\bar{1}$ 1 1)[1 $\bar{1}$ 2] |
| | (8.52, −9.95, 21.2) | ($\bar{1}$ 1 1)[1 $\bar{1}$ 2] |
| [1 1 0] | (1.45, −9.66, 6.12) | (1 1 $\bar{1}$)[1 1 2] |
| | (1.0, −9.66, −7) | (1 1 1)[$\bar{1}$ $\bar{1}$ 2] |
| [1 1 1] | (−13.37, −9.42, 9.90) | ($\bar{1}$ 1 1)[2 1 1] |
| | (13.03, −11.92, 3.67) | (1 $\bar{1}$ 1)[1 2 1] |

Indentation is along the negative $y$ direction.

One can make out eight disks, each about seven atoms across, as well as a few isolated atoms that have also moved considerably. The other images are for the other crystal orientations, but are a few CG steps later in the process, and as such we are already a little "too late" in observing the nucleation. These images were not the exact ones used to determine the value of $d_{\text{nuc}}$, but they are useful here to help visualize the slightly larger post-nucleation disks.

In Table 1, a summary of the resulting locations and types of each nucleated defect observed in the 3D simulations is provided. Note that while the very small load steps we took in the 2D simulations assured that only a single instability was observed in each, here the somewhat "large" (0.25 Å) steps mean that it is typical for more than one dislocation to nucleate simultaneously in each simulation.

We now confine our attention to the 2D simulations for the purposes of discussing the existing nucleation criteria. We will return to the 3D results in Section 4.2.

## 3. Analysis of existing criteria

In this section we look at three existing nucleation criteria and discuss the ways in which they break down. The exercise is perhaps rather long, but it emphasizes the important features of the homogeneous nucleation mechanism that the existing criteria do not seem to catch.

### 3.1. The Rice model

The model of Rice (1992) is based on the Peierls (1940) model of a dislocation and the concept of the $\gamma$-surface (Vitek et al., 1972). Rice analyzed the simplified geometry of a sharp crack in a body that was continuous and linear elastic everywhere except on a single slip plane intersecting the crack tip. Across this plane, a discontinuity in displacements is permitted. The traction on the elastic regions on either side of the planes is balanced by an atomistically based relation between the displacement discontinuity and the resulting stress. Since there is a maximum stress that is sustainable at the slip plane, it is possible to compute the conditions for which the displacement discontinuity becomes a fully formed dislocation. This model is relatively straightforward to implement in an FE framework (Reddy, 1993; Zienkiewicz and Taylor, 1989; Hughes, 1987) as follows.

We consider the 2D triangular lattice of atoms shown in Fig. 7, and connect the atoms via an FE mesh. Elements which do not intersect the chosen slip plane are modeled as linear elastic continuum elements, and thus the "atoms" defining them become FE nodes. In the usual FE way, then, the strain energy in these elements is known from the displacements of the three nodes (atoms) defining them, the linear shape functions,

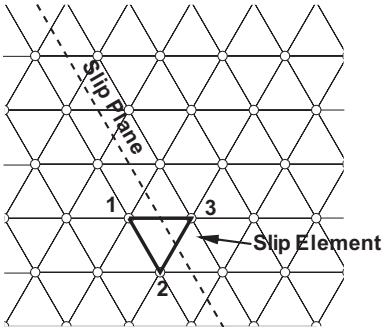


Fig. 7. A simple 2D triangular lattice and a slip plane. Elements are "slip elements" if they lie on the slip plane, or linear elastic otherwise.

and the isotropic elastic constants $E$ and $v$.[3] For elements on the slip plane, we define a new type of element that we call a "slip element". For each slip element (see the example in Fig. 7), we identify the side of the element which is parallel to the slip plane and label the two nodes comprising this side as 1 and 2. The sole node on the other side of the slip plane we call node 3, numbering anti-clockwise around the element. The reference position of node $i$ is $\boldsymbol{X}_i$ and its displacement is $\boldsymbol{u}_i$. We define a displacement discontinuity, $\boldsymbol{v}$, within the element as

$$\boldsymbol{v} = \boldsymbol{u}_3 - \frac{\boldsymbol{u}_1 + \boldsymbol{u}_2}{2}, \tag{2}$$

which we decompose into a slip component (and an opening component) by taking the projection along (and perpendicular to) the unit vector pointing from nodes 1 to 2 in the *deformed* configuration. Thus

$$\boldsymbol{s} = (\boldsymbol{X}_2 + \boldsymbol{u}_2) - (\boldsymbol{X}_1 + \boldsymbol{u}_1), \tag{3}$$

$$\hat{\boldsymbol{s}} = \frac{\boldsymbol{s}}{|\boldsymbol{s}|} \tag{4}$$

defines the unit vector pointing from nodes 1 to 2, we define $\hat{\boldsymbol{n}}$ as a unit vector normal to $\hat{\boldsymbol{s}}$, and the slip ($\Delta$) and opening ($h$) components are then

$$\Delta = \boldsymbol{v} \cdot \hat{\boldsymbol{s}}, \tag{5}$$

$$h = \boldsymbol{v} \cdot \hat{\boldsymbol{n}}. \tag{6}$$

We assume that a $\gamma$-surface is known for the system; we have a function $\gamma(\Delta, h)$ that defines the energy of slip and opening per unit area. For simplicity we take the Frenkel (1926) sinusoid for slip and a harmonic model for opening, fitted to the elastic properties of the lattice. Thus

$$\gamma(\Delta, h) = \frac{Gb^2}{4\pi^2 d}\left(1 - \cos\frac{2\pi\Delta}{b}\right) + \frac{E}{2d}h^2, \tag{7}$$

where $G = 0.5E/(1+v)$ and $d$ is the interplanar spacing. Of course, more complex forms that better reflect a real atomistic system (Kaxiras and Duesbery, 1993; Bulatov and Kaxiras, 1997) or include coupling effects between slip and opening (Sun et al., 1993) are possible. Our simple model in Eq. (7) reproduces linear elasticity for small deformations and provides a simple effect of lattice discreteness and periodicity.

Multiplying this surface energy by the area (length of $|\boldsymbol{X}_2 - \boldsymbol{X}_1|$ in 2D) of the slip plane gives the energy due to the slip distribution.[4] Since this energy can be found element-by-element from the displacements of the three nodes defining each element, these elements can naturally be mixed with the linear elastic elements of the remaining mesh and equilibrium configurations can be found by minimizing the total energy of the system under some applied load.

[3] A triangular lattice is elastically isotropic in the $x$–$y$ plane. For our model $E = 0.5272\,\text{eV}/\text{Å}^3$ and $v = 0.375$.

[4] In fact, we must also divide each contribution by a factor of 2 because of the double counting of slip plane area. Each element overlaps half of its neighbor on each side along the slip plane.

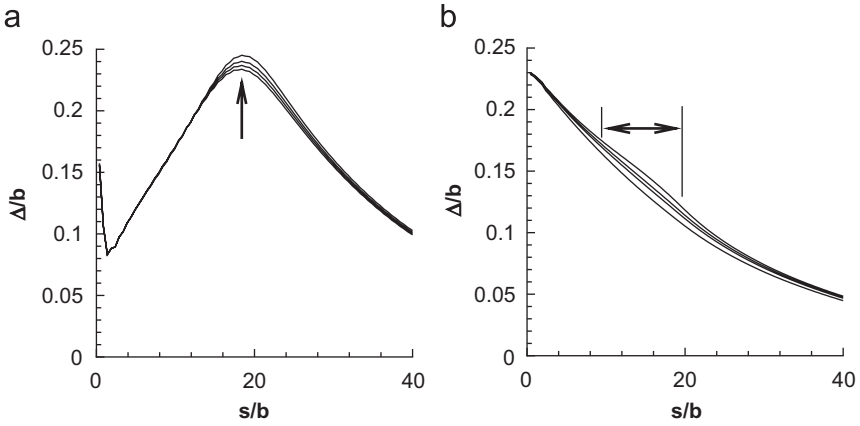


Fig. 8. Slip distributions prior to defect formation along the plane of eventual nucleation (a) for the Rice model and (b) extracted from the atomistic result. $s$ is the distance along the slip plane from the surface. Four curves for four different load levels are shown to indicate the evolution of the curve with increased load. Arrows indicate the size and location of the defect which eventually forms.

With this simple model, we can revisit the same indentation test as discussed in Section 2.1. By systematically varying the slip plane and repeating the simulation up to the nucleation, we can determine the slip plane location where the minimum indenter load is required for nucleation, and thus find the predicted location of defect formation.

This model does not correctly predict homogeneous nucleation. The first dislocation is nucleated at a much larger indentation depth than in the atomistic simulation: about $d = 46\,\text{Å}$ versus $d = 31\,\text{Å}$. Also, the location of the nucleation is six atomic planes below the correct one, which can partially be explained by the higher load sustained before nucleation: the deeper indentation depth means a larger contact area, and since the stress field will be roughly self-similar as the contact area increases, one expects the plane of nucleation to move deeper into the crystal. It is possible that one could improve this prediction using a more accurate $\gamma$-surface, or a nonlinear constitutive model away from the slip plane. However, the following observations point to a need for some form of nonlocal Peierls model (Miller et al., 1996) as well.

The Rice model allows for a very straightforward visualization of the nucleation process by monitoring the slip distribution along the slip plane in the steps prior to nucleation. In Fig. 8, we see the differences between the Rice model and the actual atomistic results. On the left, we show the Rice model's slip distribution as a function of distance from the free surface, $s$, along the slip plane. Shown are four relaxed configurations prior to nucleation, representing increments in the indenter depth of 0.5 Å. On the right, a similar set of curves are extracted from the atomistic simulations. In the Rice model, slip builds continuously and gradually on the slip plane, with a maximum value at approximately the location of the ultimate nucleated defect. When the maximum slip reaches $b/4$ (one quarter of the Burgers vector), a dipole with essentially zero diameter nucleates. The value of $b/4$ makes sense in terms of the $\gamma$-surface underlying the model: this value of $\Delta$ corresponds to the maximum stress that the slip plane can support. The real slip distribution, however, is very different and shows no obvious peak near the point of ultimate nucleation. Only a slight change in convexity can be seen in the final step before nucleation, but the defect forms long before a value of $\Delta = b/4$ is reached.

Although we have not rigorously derived or explored this statement, it seems intuitive that the criterion for nucleation in the Rice model will essentially be this: when the slip at any point reaches $\Delta = b/4$, the defect nucleates. Clearly, though, Fig. 8(b) shows that this is not what really takes place. It seems that two factors affect the Rice model's prediction. First, in the atomistic simulation it is clear that the nonlinear deformation is not confined to a single slip plane as is assumed in the Rice framework. Second, the local nature of the slip energy relation allows the Rice model to nucleate a dipole that is vanishingly small, while the atomistic system is unable to nucleate a dipole with a diameter smaller than $d_{\text{nuc}}$.

### 3.2. The atomic-scale Hill criterion

The criterion of van Vliet et al. (2003) takes the continuum treatment of bifurcation originally developed by Hill (1962), and applies it at the atomic scale. In short, the continuum model states that the matrix

$$c_{ijkl}w_iw_k - \tau_{jl} \tag{8}$$

must remain positive-definite for the material to be stable. In this expression $\boldsymbol{c}$ is the spatial, incremental elastic modulus, $\boldsymbol{\tau}$ is the Cauchy stress and $\boldsymbol{w}$ is any arbitrary unit vector. Note that the material is of course not linear elastic, rather $\boldsymbol{c}$ is the tangent modulus, i.e., the first order expansion of the material's response to *further* deformation from some instantaneous deformed state.

The check for positive-definiteness can be posed as the following eigenvalue problem:

$$(c_{ijkl}w_iw_k - \tau_{jl})k_l = \Lambda k_j, \tag{9}$$

where the material will be unstable if any of the eigenvalues $\Lambda$ are less than zero. Thus, the load level at which the minimum eigenvalue, $\Lambda_{\min}$, is less than zero somewhere in the body is the predicted onset of a material instability.

van Vliet et al. (2003) proposed a natural extension of this to the atomic scale, whereby they replaced $c_{ijkl}$ and $\tau_{jl}$ with their atomistic counterparts: the virial stress (Vitek and Egami, 1987) and the Ray (1988) expression for the moduli associated with each atom, $I$. Thus, they computed:

$$\Lambda^I = (c^I_{ijkl}w_iw_k - \tau^I_{jl})k_lk_j, \tag{10}$$

for each atom $I$, scanning over all possible vectors $\boldsymbol{w}$ and $\boldsymbol{k}$ to find $\Lambda^I_{\min}$. Their criterion was then that nucleation would occur at the location of the atom where $\Lambda_{\min}$ first approached zero. The corresponding $\boldsymbol{k}_{\min}$ and $\boldsymbol{w}_{\min}$ predict the slip plane normal and Burgers vector, respectively, of the nucleated defect.

van Vliet et al. (2003) examined their criterion using a 2D triangular lattice similar to the one studied here, except with a simpler interatomic potential. Specifically, they used a Fermi–Pasta–Ulam (FPU) near-neighbor pair potential model to reproduce bubble raft results. This potential is of the form

$$V(r) = \varepsilon\left[\left(\frac{1-\tilde{r}}{1-x}\right)^4 - 2\left(\frac{1-\tilde{r}}{1-x}\right)^2\right], \tag{11}$$

where $x = 0.85$ was selected and $\tilde{r} = r/r_{\text{cut}}$ where $r_{\text{cut}}$ is the cutoff radius of the potential (for $r > r_{\text{cut}}$ it is set identically to zero). This potential has the property that the equilibrium triangular lattice constant is $a_0 = xr_{\text{cut}}$ and the cohesive energy is $3\varepsilon$. To be able to make easy comparisons with the Al EAM model used earlier, we choose $r_{\text{cut}} = 3.329\,\text{Å}$ so that the two models give the same lattice constant, and set $\varepsilon = 1\,\text{eV}$ arbitrarily. For conciseness, we refer to two 2D materials: Al refers to our EAM model and FPU refers to the pair potential of Eq. (11).

As shown by Li et al. (2002), the criterion works very well when the FPU crystal is indented along [0 1]. It accurately identifies the location and type of defect which nucleates, as shown in Fig. 9(a) (showing the last stable configuration before nucleation). Just before nucleation, $\Lambda_{\min} = 8\,\text{eV/Å}^3$, or about 8% of the value of $96\,\text{eV/Å}^3$ found in the perfect crystal. However, the criterion is not as robust for the Al model. Although the location and type of defect is correctly predicted by the minimum value of $\Lambda_{\min}$, the value is $-0.1234\,\text{eV/Å}^3$, a significantly *negative* number compared to the value of $3.93\,\text{eV/Å}^3$ found in the perfect crystal. The empty region in the center of Fig. 9(b) is the region in which $\Lambda_{\min}$ is negative, even though the crystal remains stable. While this seems like a small discrepancy, it means that the criterion loses its conceptual framework, which in the continuum setting was based on a clear connection between loss of positive-definiteness and instability. In the atomistic analogy, this connection is lost, and there is no clear choice for the critical value of $\Lambda_{\min}$. This again points to the importance of *nonlocality* in the atomistic system. The atomic quantities $c^I_{ijkl}$ and $\tau^I_{jl}$ are essentially local quantities, defined in terms of a single atom (and its neighbors), but the nucleation process involves a large number of atoms moving collectively, and cannot be predicted by a quantity based on a single atom alone.

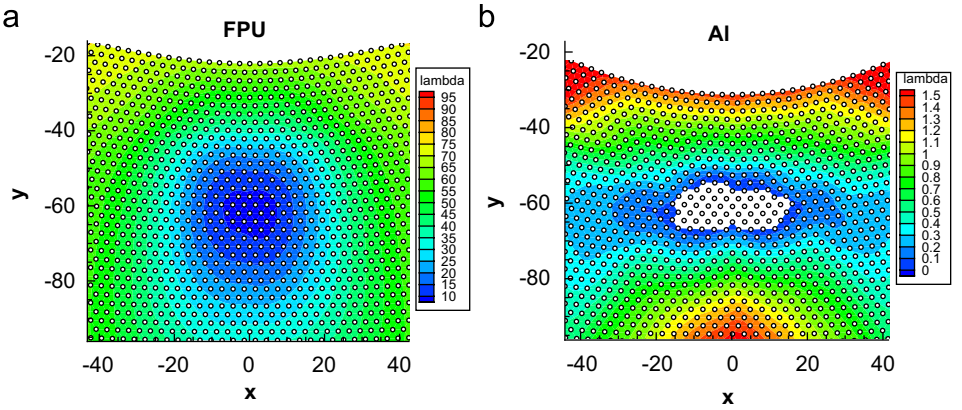


Fig. 9. Predictions of the atomic-scale Hill criterion for (a) FPU and (b) Al. The empty region in the center of (b) is the region where $\Lambda_{\min}$ is less than zero.

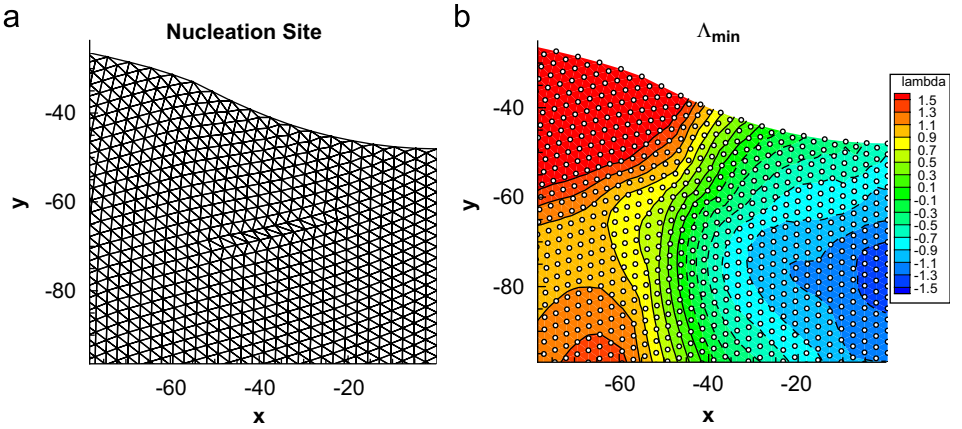


Fig. 10. (a) Nucleation of a dislocation in a triangular lattice of Al indented along [0 1]. (b) Predictions of the atomic-scale Hill criterion for the same simulation. Dashed lines highlight contours which are negative values of $\Lambda_{\min}$.

The situation is worse when we change the orientation of the Al crystal via a 90° rotation, and try the indentation along the [1 0] direction shown in Fig. 1. In Fig. 10(a), we show the initial stage of nucleation via the deforming mesh between the atoms. We show only the left side, since in this case two defects nucleate simultaneously at locations symmetric with respect to the center line. In Fig. 10(b), we show the contours of $\Lambda_{\min}$, which are also symmetric about the centerline, for the last equilibrium configuration prior to nucleation. We see that the problem of finding $\Lambda<0$ before nucleation persists, and also that the location of $\Lambda_{\min}$ is in this case incorrect: it occurs on the centerline rather than at the correct locations of $x \approx \pm 40$ Å.

These observations beg the question of why the simplified FPU material does not seem to have these problems, and the explanation is again enlightening in the context of the importance of nonlocality. The FPU model is a near-neighbor pair potential model. That is to say, it is only very weakly nonlocal, since an atom's energy and stress are determined by the minimal interaction range that an atomistic model can have. For the longer-ranged and environmentally dependent EAM Al model, the nonlocality is much more important and leads to the failure of the criterion.

van Vliet et al. (2003) noted other limitations of their model. Specifically, they need to explicitly disregard regions near topological defects (e.g., free surfaces, grain boundaries) or near pre-existing dislocations, where $\Lambda$ can be less than zero even though no subsequent nucleation will occur. One of our goals here is to develop a criterion which is correct even in the presence of such defects.

### 3.3. The Miller/Acharya criterion

Miller and Acharya (2004) developed a criterion based on nonequilibrium dislocation field theory, arguing that, to a rough approximation, the thermodynamic driving force for dislocation nucleation at a point is proportional to the curl of the stress at that point. The scalar quantity

$$N_{m,l} = |\boldsymbol{m} \cdot \nabla \times \sigma \cdot \boldsymbol{l}| \tag{12}$$

is then the quantity related to nucleation of a dislocation with Burgers vector directed along $\boldsymbol{m}$ and line direction $\boldsymbol{l}$. They then postulated that there is a critical value for a given crystal, $N_{\text{crit}}$, such that a dislocation will nucleate when $N_{m,l} = N_{\text{crit}}$.

To extend this continuum notion to the atomic scale, they followed a similar strategy to van Vliet et al. (2003), which is to replace the continuum stress by the virial stress at each atom. They then computed the curl in an approximate way using an FE interpolation of the stress values between the atoms.

Unfortunately, this criterion suffers from similar deficiencies to those found with the atomic-scale Hill criterion. For the indentation of a triangular lattice along the [0 1] direction, the prediction is reasonably accurate (Miller and Acharya, 2004), but for crystal orientations where the dislocation nucleates off the axis of the indentation, the agreement is not good. To try and improve this agreement, Miller and Acharya tried to examine the value of $N_{m,l}$ for nonequilibrated configurations of atoms *during* the CG minimization of the critical load step. But a truly useful criterion must be able to make predictions based on equilibrated states at load levels below the critical ones.

Much like the atomic-scale Hill criterion, the criterion of Miller and Acharya does not work near topological defects or near pre-existing dislocations: for example the value of $N_{m,l}$ can be greater than $N_{\text{crit}}$ inside dislocation cores and near unstressed free surfaces.

We note that while the theory providing the foundations of the Miller/Acharya criterion is inherently nonlocal, the definition of the stress at the atomic scale is local in that Miller/Acharya used the usual virial form extended to the scale of a single atom. Once again, it seems that the use of this local, atom-by-atom quantity cannot successfully predict nucleation by the collective motion of a large number of atoms. It is possible that some modified definition of the atomic-level stress, most likely one that is based on a nonlocal (Eringen, 1987) or second-gradient continuum theory (Sunyk and Steinmann, 2003; Shibutani et al., 1998; Chen et al., 2004), could improve the Miller/Acharya criterion (a similar statement can be made about the atomic-scale Hill criterion). Thus far, we have been unable to find a suitable modification to the atomic level concepts of stress and moduli that serve to repair either criterion's limitations.

## 4. The new criterion

To build a new criterion, we start from the conceptual framework of the atomic-scale Hill model. That is to say, we adopt the view that local loss of stability can be used as a predictor of nucleation, and that this loss of stability can be traced to loss of positive-definiteness in some suitable stiffness matrix. However, we choose to start from fully atomistic considerations, and in that sense we are working more in the spirit of phonon stability analysis. Armed with a detailed understanding of the nucleation mechanism described above, we try to incorporate, *from the start*, the physical features of nucleation that we have observed. That is to say, we will build into our model the collective rigid sliding of two finite atomic disks, one over the other.

We denote a configuration by the vector $\boldsymbol{x}$, of length $3N$ containing the positions of the $N$ atoms. $E(\boldsymbol{x})$ is the total energy of the configuration. For a given configuration to be in equilibrium, the force $-\partial E/\partial x_i$ must be zero for every atomic coordinate, $i$. Likewise, for this to be a *stable* equilibrium, any small arbitrary perturbation of the atomic positions must return to the equilibrium configuration upon relaxation, i.e., the *second* derivative of the energy with respect to the atomic positions must be positive-definite:

$$C_{ij} \equiv \frac{\partial^2 E(\boldsymbol{x})}{\partial x_i \partial x_j}. \tag{13}$$

$C_{ij}$ is the *atomistic acoustic tensor* of the system. In passing, we note that for most interatomic potential forms the expressions for $C_{ij}$ are easily obtained and expressed analytically. For EAM, for example, they can be found in Miller (1997).

The eigenvectors $\boldsymbol{\eta}$ of $C_{ij}$ are found from

$$C_{ij}\boldsymbol{\eta}_j = \Lambda\boldsymbol{\eta}_i, \tag{14}$$

where each $\boldsymbol{\eta}$ has a corresponding eigenvalue, $\Lambda$. Throughout this discussion we assume all eigenvectors to be normalized such that

$$\boldsymbol{\eta}\cdot\boldsymbol{\eta} = 1. \tag{15}$$

We denote the *minimum* eigenvalue by $\hat{\Lambda}$ and the corresponding eigenvector as $\hat{\boldsymbol{\eta}}$. Physically $\hat{\boldsymbol{\eta}}$ corresponds to a displacement vector from the atomic configuration $\boldsymbol{x}$. We know from the properties of symmetric matrices that $C_{ij}$ is positive-definite if $\hat{\Lambda} > 0$.

In principle, a completely general (if not especially practical) criterion for defect nucleation is simply this: One computes the minimum eigenvalue of $C_{ij}$, which at the onset of an instability will go to zero. One can then examine the corresponding eigenvector $\hat{\boldsymbol{\eta}}$ and determine the nature of the instability, which will initially correspond to the collective motion of the atoms in the direction of $\hat{\boldsymbol{\eta}}$. If the instability corresponds to the nucleation of a dislocation, the eigenvector will necessarily look something like Fig. 4(c), and thus we can determine by inspection the slip plane and Burgers vector of the forming dipole.

There are two practical difficulties with this "criterion" as just stated. First, we cannot expect to diagonalize a $3N \times 3N$ matrix at each time step in an $N$ atom simulation for even moderately sized $N$. Second, while the analysis would tell us *when* the system became unstable, it would not tell us *where*, nor will it tell us the type of nucleated defect, without the difficult task of examining the eigenmode.

However, the localized nature of the nucleation, which we contend is mostly confined to a small disk of atoms on only two adjacent planes, permits us to define a spatially varying acoustic tensor of much smaller dimension. For example, imagine we define a region around an atom $I$ at the center of a nucleation site like the one shown in Fig. 4, and build a submatrix of $C_{ij}$, called $C^I_{ij}$, that includes only terms of $C_{ij}$ between the $M$ atoms inside the region. We expect that for some relatively large region, the submatrix $C^I_{ij}$ will have virtually the same minimum eigenvalue and corresponding eigenvector as $C_{ij}$, since we saw that the eventual motion of the atoms far from the nucleation site was essentially zero anyway. More importantly, it is clear that if $C^I_{ij}$ is not positive-definite, then neither is the full matrix $C_{ij}$. To see this, assume that $C^I_{ij}$ is not positive-definite. There exists, therefore an eigenvector of $C^I_{ij}$, $\hat{\boldsymbol{\eta}}^I$, with eigenvalue $\hat{\Lambda}^I < 0$. We rearrange the rows and columns of the full matrix $C_{ij}$ such that $C^I_{ij}$ resides in the top left corner, and define the vector $\boldsymbol{\xi}$ as

$$\boldsymbol{\xi} = [\hat{\boldsymbol{\eta}}^I, \underline{0}]. \tag{16}$$

It is clear that

$$\xi_i C_{ij}\xi_j = \hat{\eta}^I_i C^I_{ij}\hat{\eta}^I_j = \hat{\Lambda}^I < 0, \tag{17}$$

and therefore $C_{ij}$ is not positive-definite. Thus, a sufficient (but not necessary) condition for loss of stability of $C_{ij}$ is that any submatrix $C^I_{ij}$ is not positive-definite. The question which remains is what is the smallest region we can consider around each point, $I$.

We now make use of the observed nucleation mechanism. Specifically, we define a submatrix centered on every atom $I$ that takes on the characteristics of the defect nucleation disk for slip plane $p$, as illustrated in Fig. 11. This is the region shown earlier in Fig. 4, where we have highlighted one atom, $I$. We define a "disk" of atoms (two rows in 2D), two planes thick and of some fixed diameter. The diameter of the disk should obviously be large enough to capture the full critical disk, which depends on indenter size. In our simulations, we focus on $R = 100$ Å, and so from Fig. 5(a) we fix the disk diameter at $d = 28$ Å. Making the disk larger, and thereby being conservative in terms of the number of atoms we include does not change the results significantly. On the other hand, making the disk smaller than the critical nucleating disk will lead to poor results.

For each disk, we extract the elements of $C_{ij}$ for which both $i$ and $j$ correspond to atoms within the disk and build the submatrix $C^{I,p}_{ij}$. We can now compute the minimum eigenvalue $\hat{\Lambda}^{I,p}$ and eigenvector $\hat{\eta}^{I,p}$ of $C^{I,p}_{ij}$ for

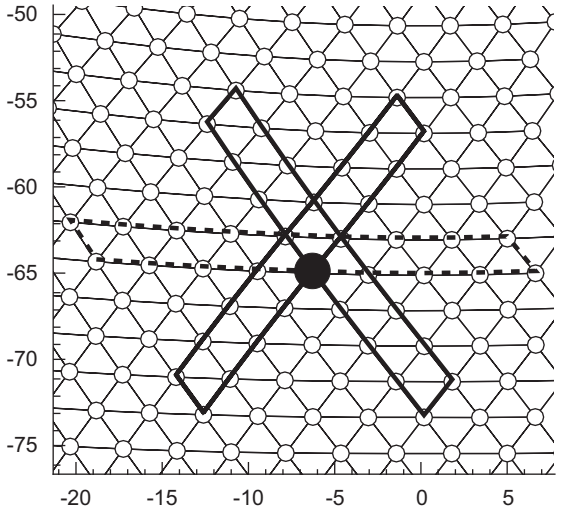


Fig. 11. The disks used to define $C^{I,p}$ for the bold atom $I$ on each of the three possible slip planes $p$.

every atom $I$ and slip plane $p$,

$$C_{ij}^{I,p}\hat{\eta}_j^{I,p} = \hat{\Lambda}^{I,p}\hat{\eta}_i^{I,p}. \tag{18}$$

We make the hypothesis that *nucleation will occur when any* $\hat{\Lambda}^{I,p} \leqslant 0$*, and it will be centered at the location of the corresponding atom I, on slip plane p*. In the 2D example, there is only one slip system on each slip plane, and thus this will immediately predict the Burgers vector as well. However, in 3D there are three slip systems per slip plane and $\hat{\Lambda}^{I,p}$ will not be able to resolve between them. To predict the Burgers vector of the dislocation that forms, we need to examine the nature of the eigenvector $\hat{\boldsymbol{\eta}}^{I,p}$. From Fig. 4, we know $\hat{\boldsymbol{\eta}}^{I,p}$ is well-approximated by a vector for which all the atoms on one side of the disk move the same amount, $\Delta_\mu$, along the slip direction (where $\mu$ denotes a specific slip system in the plane $p$) while all the atoms on the other side move $-\Delta_\mu$. Thus we define a vector $\boldsymbol{b}^\mu$ for each possible Burgers vector $\mu$ consistent with this simplified model of the nucleation process. The vector contains entries that are either $\Delta_\mu$ or $-\Delta_\mu$ as appropriate, with the magnitude of $\Delta_\mu$ chosen to normalize $\boldsymbol{b}^\mu$. We expect that $\hat{\boldsymbol{\eta}}^{I,p}$ should closely approximate one of these $\boldsymbol{b}^\mu$, thus determining the slip direction. Next we define

$$K_\mu(\boldsymbol{x}_I) = \frac{\hat{\Lambda}^{I,p}}{|\boldsymbol{b}^\mu \cdot \hat{\boldsymbol{\eta}}^{I,p}|}. \tag{19}$$

The effect of the denominator, which is between 0 and 1, is to resolve the degeneracy between slip systems $\mu$ on the same plane, $p$. Thus the final form of our criterion is to postulate that *the smallest value of* $K_\mu(\boldsymbol{x}_I)$ *predicts nucleation of a dislocation loop on slip system* $\mu$ *at position* $\boldsymbol{x}_I$. Note that by the absolute value taken and through the normalization of $\boldsymbol{b}^\mu$ and $\hat{\boldsymbol{\eta}}^{I,p}$, the denominator does not change the critical value of $K$, which is $K = 0$.

The criterion can be implemented for large numbers of atoms $N$ without the need for $N^2$ storage of the full stiffness matrix $\boldsymbol{C}$ or the $N^3$ time required to diagonalize it. Since the number of atoms in the disk used to build the submatrices $\boldsymbol{C}^{I,p}$ is fixed to $M \ll N$, the time to evaluate the criterion everywhere in a simulation scales as $M^3N$ where $M$ is a constant. Moreover, since there is much overlap between the submatrices $\boldsymbol{C}^{I,p}$ within $\boldsymbol{C}$, storing entries as they are computed and retrieving them using a binary tree (Knuth, 1968) can substantially speed-up the calculations. Finally, since $K$ varies smoothly from atom to atom, we find that we can omit the calculation of atom $I$ if one of its nearest neighbors has already been considered. This reduces somewhat the spatial resolution of our results, to about the near-neighbor distance.

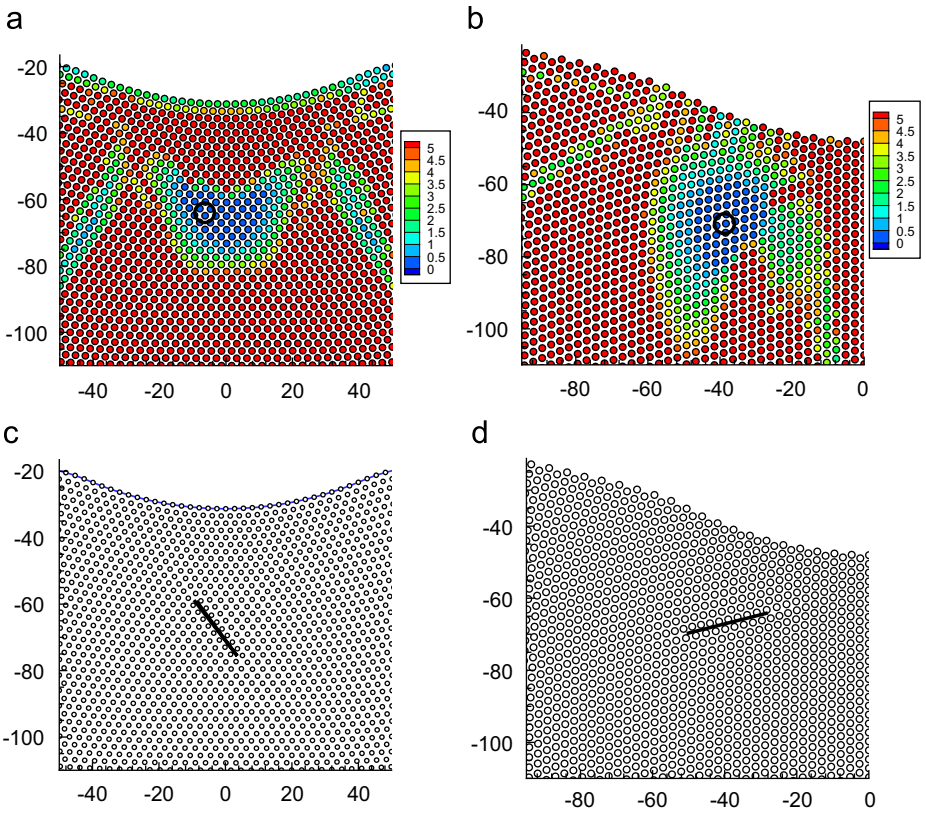


Fig. 12. $K_{\min}$ for indentation along (a) [0 1] and (b) [1 0], compared to the observed location on dislocation nucleation in (c) [0 1] and (d) [1 0]. Predictions of the criterion in (a) and (b) are in exact agreement with the actual location and type of nucleated defects in (c) and (d).

### 4.1. 2D predictions

In Fig. 12 we show the predictions of the criterion for two 2D simulations: indentation along [0 1] and [1 0] in Al. In (a) and (b), the atoms are colored according to their values of $K_{\min} = \min(K_1, K_2, K_3)$, and the atom with the lowest value is circled. In (c) and (d), the actual nucleation site is shown, which we see matches exactly with the criterion. The slip system predicted is also correct in both cases. An interesting feature of the [1 0] results plotted in (a) is the region of low values of $K$ on the left and right of the actual nucleation site (near, for example $(x, y) = (-45, -75)$). These correspond to regions where defects of the type formed in the [0 1] indentation are incipient, but do not get a chance to form before the defect in the center removes the driving force on these other areas. Note also that the values of $K$ in these outer regions are low, but not as low as those appearing in the correct nucleation site. In no case have we found the value of $K$ to drop below zero in an equilibrium configuration of atoms, leaving intact our conceptual framework that such a value can only appear in an unstable state.

Fig. 13 shows $K_\mu$ for each of the three slip systems separately for the [1 0] indentation, instead of the minimum of the three as shown in Fig. 12(b). The two inclined slip planes have more or less symmetric distributions of $K$, with minima at the correct locations in the crystal. The third slip system (with planes oriented vertically in this case) has two regions of low $K$ somewhat further away from the centerline. This value of $K$ is not as low as the value at the actual location of defect nucleation, but is consistent with other simulations of nanoindentation (Dupuy et al., 2005; Miller and Acharya, 2004) on systems where the active slip planes are vertical relative to the indentation direction.

In Fig. 14 we show the values of $K$ for the first equilibrium configuration *after* a dislocation has nucleated. The nucleated dislocation has come to rest inside the circle on the upper left side (the other half of the dipole has moved down and to the right, out of view). This figure and the previous (Fig. 12(a)) illustrate two

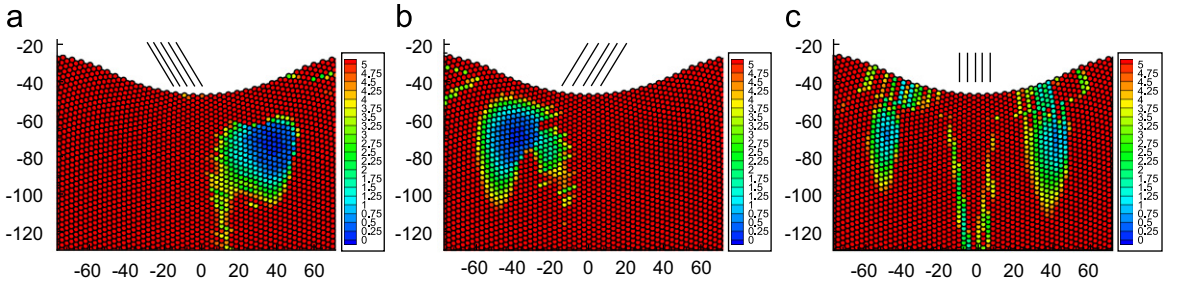


Fig. 13. The values of $K_\mu$ for $\mu$ corresponding to the three different slip systems during indentation along [1 0] in a triangular lattice. The slip plane corresponding to $\mu$ is shown above each image.

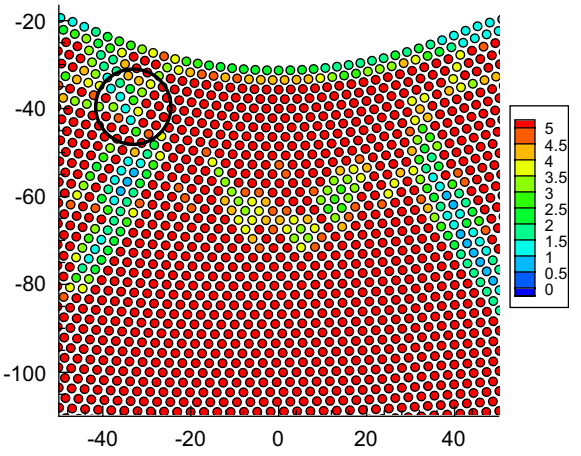


Fig. 14. After nucleation, there are no predicted locations of further nucleation, neither at free surfaces nor in the pre-existing dislocation core shown at the circle.

important features of the criterion. First, the value of $K$ is neither near nor below the critical value inside the dislocation core, thus no special treatment is required in the presence of existing defects. Second, although $K$ is somewhat lower at the free surface than in the bulk, it is not critically so, and again no special treatment of topological defects like a free surface is required.

Note that the criterion naturally extends to nucleation at a point of stress concentration near a free surface. For atoms near a surface, the "disk" extends beyond the surface, and thus no atoms are found at some disk sites. Thus, in the limit of an atom on the surface, the actual atoms used in forming $\boldsymbol{C}^{I,p}$ are those contained in half of a disk extending to one side of atom $I$ and into the crystal. It seems plausible that the formation of a loop from the surface would in fact start from such a nucleus, and recent results by Li (2007) suggest this behavior. We have performed indentation simulations using a flat punch instead of the spherical indenter to force nucleation to occur at the surface, and found that our criterion remains robust in predicting the surface nucleation.

In Fig. 15 we show the minimum value of $K$ in the "bulk" regions away from the free surfaces as a function of indenter displacement. In the initial perfect crystal, the bulk value of $K$ is about $32\,\mathrm{eV}/\mathrm{\AA}^2$ and sets the scale for what constitutes a "small" value of $K$. Along the surface, the value of $K$ remains near about $1\,\mathrm{eV}/\mathrm{\AA}^2$ throughout the indentation, a relatively small value but still distinguishable from the value at the nucleation site which is $0.148\,\mathrm{eV}/\mathrm{\AA}^2$.

### 4.2. 3D predictions

In Table 2 we summarize the location and type of defects predicted by the criterion. In all cases, the predicted types are correct and consistent with what we summarized in Table 1, or else they are predictions for

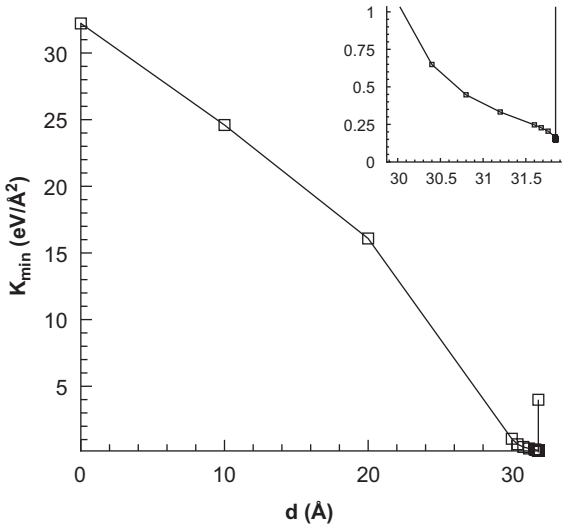


Fig. 15. The minimum value of $K$ in the critical region below the indenter versus indenter displacement, for the indentation into Al in the [1 0] direction. The inset shows the final stages of loading.

Table 2
Predicted locations (relative to the initial point of indenter contact at $(0,0,0)$) and types of nucleated defects in the 3D simulations

| Indent dir'n | Disl. location (Å) | Disl. type | $\Delta x$ (Å) |
|---|---|---|---|
| [1 0 0] | (−21.29, −13.33, 8.34) | (1 1 1)[$\bar{1}$ $\bar{1}$ 2] | 2.76 |
| | (8.34, −13.32, −21.29) | (1 1 1)[$\bar{1}$ $\bar{1}$ 2] | 2.77 |
| | (21.28, −13.32, 8.34) | (1 $\bar{1}$ 1)[$\bar{1}$ 1 2] | 5.52 |
| | (−8.35, −13.32, −21.29) | (1 $\bar{1}$ 1)[$\bar{1}$ 1 2] | 4.23 |
| | (21.17, −9.77, −8.46) | (1 1 $\bar{1}$)[1 1 2] | 2.57 |
| | (−8.46, −9.77, 21.17) | (1 1 $\bar{1}$)[1 1 2] | 2.76 |
| | (−21.29, −13.33, −8.35) | ($\bar{1}$ 1 1)[1 $\bar{1}$ 2] | 4.24 |
| | (8.34, −13.32, 21.28) | ($\bar{1}$ 1 1)[1 $\bar{1}$ 2] | 3.38 |
| [1 1 0] | (1.13, −9.82, 5.52) | (1 1 $\bar{1}$)[1 1 2] | 0.7 |
| | (−1.87, −9.82, −6.48) | (1 1 1)[$\bar{1}$ $\bar{1}$ 2] | 1.03 |
| [1 1 1] | (−11.27, −9.40, 7.30) | ($\bar{1}$ 1 1)[2 1 1] | 3.34 |
| | (11.63, −9.30, 7.60) | (1 $\bar{1}$ 1)[1 2 1] | 4.93 |
| | (−0.07, −9.50, −12.70) | ($\bar{1}$ $\bar{1}$ 1)[1 1 2] | Not nuc'd |

$\Delta x$ is the error in the location of the nucleation site, if in fact the dislocation was observed in Table 1.

one of the symmetric locations illustrated in Fig. 6 but not actually observed in the indentation simulation. These "missing" defects are presumably excluded due to other defects nucleating first (due to slight asymmetries in the loading and numerical noise). In the last column $\Delta x$ is the distance from the observed center of the nucleated disk to the location predicted by the criterion. The resolution of the predicted location is about a near-neighbor distance due to the reduced sampling. There is also an uncertainty in the exact location of the center of the observed defect (determined by eye), again on the order of a near-neighbor distance. Within these uncertainties, the predicted locations are exactly correct.

## 5. Summary and future directions

We have performed lattice static simulations of nanoindentation in 2D and 3D to reveal the exact details of the mechanism of homogeneous dislocation nucleation. For the materials studied here (a model triangular

lattice in 2D and an fcc lattice in 3D), the nucleation mechanism is always the same: the formation of a glissile Shockley partial shear loop in fcc or a dipole of shear dislocations in 2D. In all cases, the initial nucleus of the dislocation has a finite diameter, which depends approximately linearly on the size of the indenter. We find that there is very little dependence of the hardness at nucleation on the indenter radius, which is very different from the inverse square-root dependence of the ISE.

We have systematically considered three nucleation criteria from the literature and concluded that they are limited due to their local nature. The finite size of the nucleated defects we observe indicates an inherently nonlocal process dependent on many atoms. On the other hand, the continuum-based criteria are all local in their formulation, using quantities defined point-wise (or atom-by-atom). We believe that this is the source of the failure of the nucleation criteria.

We then presented an atomistically based criterion that utilizes spatially varying submatrices of the atomistic acoustic tensor. The criterion is thus inherently nonlinear and nonlocal. Our approach works well in 2D and 3D, as well as in the presence of topological defects like free surfaces and pre-existing dislocation cores.

The main disadvantage of the presented criterion is that it is not clear how it can be used in larger-scale continuum models like discrete dislocation dynamics simulations (see, for example, Fivel and Canova, 1999 or van der Giessen and Needleman, 1995). There is no obvious connection between a readily accessible continuum quantity (like stress or strain) and the submatrix of the acoustic tensor that we have shown to be an accurate predictor of nucleation. This suggests that *local* continuum mechanics is not likely to be adequate to formulate a nucleation criterion. Instead, a fruitful direction of study seems to be to develop connections between atomistic models and higher-order continuum theories. Specifically, nonlocal continuum mechanics (Eringen, 1987), or gradient theories (Sunyk and Steinmann, 2003; Shibutani et al., 1998; Chen et al., 2004) seem to be the theories possessing the minimum level of sophistication to have a chance of success.

Another important aspect of nucleation, of course, is the role of thermal fluctuations. Clearly, finite temperature nucleation processes will be governed by the ability of the system to escape local energy minima. The activation barriers associated with nucleation will be dependent on the force applied to the indenter, the indenter size, and the remote boundary conditions. Calculation of such barriers is a challenging problem, but may be obtainable with saddle-point search methods (Olsen et al., 2004; Henkelman and J'ohannesson, 2000), or accelerated dynamic methods such as those developed by Voter (1997) and Sørensen and Voter (2000).

## Acknowledgments

The authors would like to thank Jim Rice, Amit Acharya, Samuel Forest and Ellad Tadmor for many useful discussions surrounding this work. The authors are grateful to the CNRS (''post rouge''), the INP Grenoble, the France-Canada Research Foundation and the French Embassy in Canada for the funding that made this work possible.

## References

Born, M., Huang, K., 1954. Dynamical Theory of Crystal Lattices. Clarendon, Oxford.

Bulatov, V., Kaxiras, E., 1997. Semidiscrete variational peierls framework for dislocation core properties. Phys. Rev. Lett. 78 (22), 4221–4224.

Chen, Y., Lee, J.D., Eskandarian, A., 2004. Atomistic viewpoint of the applicability of microcontinuum theories. Int. J. Solids Struct. 41, 2085–2097.

Chiu, Y., Ngan, A., 2002. Time-dependent characteristics of incipient plasticity in nanoindentation of a $Ni_3Al$ single crystal. Acta Mater. 50 (6), 1599–1611.

Christopher, D., Smith, R., Richter, A., 2001. Atomistic modelling of nanoindentation in iron and silver. Nanotechnology 12, 372–383.

Corcoran, S.G., Colton, R.J., Lilleodden, E.T., Gerberich, W.W., 1997. Anomalous plastic deformation at surfaces: nanoindentation of gold single crystals. Phys. Rev. B 55 16057–+.

de la Fuente, O.R., Zimmerman, J., Gonzalex, M., de la Figuera, J., Hamilton, J., Pai, W.W., Rojo, J.M., 2002. Dislocation emission around nanoindentations on a (0 0 1) fcc metal surface studied by scanning tunneling microscopy and atomistic simulations. Phys. Rev. Lett. 88 (3), 036101.

Dobson, M., Elliott, R.S., Luskin, M., Tadmor, E.B., 2007. A multilattice quasicontinuum for phase transforming materials: cascading Cauchy born kinematics. Sci. Model Simul. (2008), in press.

Dupuy, L., Tadmor, E., Miller, R., Phillips, R., 2005. Finite temperature quasicontinuum: molecular dynamics without all the atoms. Phys. Rev. Lett. 95, 060202.
Ercolessi, F., Adams, J., 1994. Interatomic potentials from first-principles calculations—the force-matching method. Europhys. Lett. 26, 583.
Eringen, A., 1987. Theory of nonlocal elasticity and some applications. Res. Mech. 21, 313–342.
Fivel, M., Canova, G., 1999. Developing rigorous boundary conditions to simulations of discrete dislocation dynamics. Modeling Simul. Mater. Sci. Eng. 7 (5), 753–768.
Frenkel, J., 1926. Zur theorie der elastizitätsgrenze und der festigkeit kristallinischer körper. Z. Phys. 37, 572.
Gerberich, W., Tymiak, N., Grunlan, J., Horstemeyer, M., Baskes, M., 2002. Interpretations of indentation size effects. J. Appl. Mech. 69, 433–442.
Gerberich, W.W., Nelson, J.C., Lilleodden, E.T., Anderson, P., Wyrobek, J.T., 1996. Indentation induced dislocation nucleation: the initial yield point. Acta Mater. 44 (9), 3585–3598.
Henkelman, G., J'ohannesson, G., J'onsson, H., 2000. Methods for finding saddle points and minimum energy paths. In: Progress on Theoretical Chemistry and Physic. Kluwer Academic Publishers, Dordrecht, pp. 269–300.
Hill, R., 1962. Acceleration waves in solids. J. Mech. Phys. Solids 10, 1.
Hughes, T.J.R., 1987. The Finite Element Method: Linear Static and Dynamic Finite Element Analysis. Prentice-Hall, Englewood Cliffs, NJ.
Kaxiras, E., Duesbery, M.S., 1993. Free energies of generalized stacking faults in silicon and implications for the brittle–ductile transition. Phys. Rev. Lett. 70 (24), 3752–3755.
Kelchner, C.L., Plimpton, S., Hamilton, J., 1998. Dislocation nucleation and defect structure during surface indentation. Phys. Rev. B 58 (17), 11085–11088.
Knap, J., Ortiz, M., 2001. An analysis of the quasicontinuum method. J. Mech. Phys. Solids 49, 1899–1923.
Knap, J., Ortiz, M., 2003. Effect of indenter-radius size on Au(0 0 1) nanoindentation. Phys. Rev. Lett. 90, 226102.
Knuth, D.E., 1968. The Art of Computer Programming, first ed., vol. 3. Addison-Wesley, Reading, MA, USA.
Li, J., 2007. The mechanics and physics of defect nucleation. Mater. Res. Soc. Bull. 32, 151–159.
Li, J., van Vliet, K., Zhu, T., Yip, S., Suresh, S., 2002. Atomistic mechanisms governing elastic limit and incipient plasticity in crystals. Nature 418, 307–310.
Li, J., Zhu, T., Yip, S., van Vliet, K.J., Suresh, S., 2004. Elastic criterion for dislocation nucleation. Mater. Sci. Eng. A 365, 25–30.
Lilleodden, E.T., Zimmerman, J.A., Foiles, S.M., Nix, W.D., 2001. An experimental and computational study of the elastic-plastic transition in thin films. In: Material Research Society Symposium Proceedings, vol. 673, pp. P1.3.1–P1.3.6.
Lilleoden, E., Zimmerman, J., Foiles, S., Nix, W., 2003. Atomistic simulations of elastic deformation and dislocation nucleation during nanoindentation. J. Mech. Phys. Solids 51, 901–920.
Mason, J.K., Lund, A.C., Schuh, C.A., 2006. Determining the activation energy and volume for the onset of plasticity during nanoindentation. Phys. Rev. B 73 (5) 054102–+.
Miller, R.E., 1997. On the generalization of continuum models to include atomistic features. Ph.D. Thesis, Brown University.
Miller, R., Acharya, A., 2004. A stress-gradient based criterion for dislocation nucleation in crystals. J. Mech. Phys. Solids 52 (7), 1507–1525.
Miller, R., Phillips, R., Beltz, G., Ortiz, M., 1996. A non-local formulation of the Peierls dislocation model. J. Mech. Phys. Solids 46 (10), 1845–1868.
Miller, R.E., Shilkrot, L.E., Curtin, W., 2003. A coupled atomistic and discrete dislocation plasticity simulation of nano-indentation into single crystal thin films. Acta Mater. 52 (2), 271–284.
Nix, W., Gao, H., 1998. Indentation size effects in crystalline materials: a law for strain gradient plasticity. J. Mech. Phys. Solids 46, 411–425.
Olsen, R.A., Kroes, G.J., Henkelman, G., Arnaldsson, A., Jónsson, H., 2004. Comparison of methods for finding saddle points without knowledge of the final states. J. Chem. Phys. 121, 9776–9792.
Peierls, R.E., 1940. The size of a dislocation. Proc. Phys. Soc. London 52, 34.
Ray, J., 1988. Elastic constants and statistical ensembles in molecular dynamics. Comput. Phys. Rep. 8 (3), 109–152.
Reddy, J., 1993. An Introduction to the Finite Element Method, second ed. McGraw-Hill, New York.
Rice, J.R., 1992. Dislocation nucleation from a crack tip: an analysis based on the peierls concept. J. Mech. Phys. Solids 40, 239.
Rice, J.R., Beltz, G.E., 1994. The activation energy for dislocation nucleation at a crack. J. Mech. Phys. Solids 42, 333–360.
Rodney, D., 2004. Molecular dynamics simulation of screw dislocations interacting with interstitial frank loops in a model fcc crystal. Acta Mater. 52, 607–614.
Schuh, C., Mason, J., Lund, A., 2005. Quantitative insight into dislocation nucleation from high-temperature nanoindentation experiments. Nature Mater. 4 (8), 617–621.
Shenoy, V.B., Miller, R., Tadmor, E., Rodney, D., Phillips, R., Ortiz, M., 1999. An adaptive methodology for atomic scale mechanics: the quasicontinuum method. J. Mech. Phys. Solids 47, 611–642.
Shenoy, V.B., Phillips, R., Tadmor, E.B., 2000. Nucleation of dislocations beneath a plane strain indenter. J. Mech. Phys. Solids 48, 649–673.
Shibutani, Y., Vitek, V., Bassani, J., 1998. Nonlocal properties of inhomogeneous structures by linking approach of generalized continuum to atomistic model. Int. J. Mech. Sci. 40, 129–137.
Sørensen, M.R., Voter, A.F., 2000. Temperature-accelerated dynamics for simulation of infrequent events. J. Chem. Phys. 112, 9599–9606.

Steinmann, P., Elizondo, A., Sunyk, R., 2007. Studies of validity of the Cauchy Born rule by direct comparison of continuum and atomistic modelling. Modelling Simul. Mater. Sci. Eng. 15 271–+.

Sun, Y., Beltz, G.E., Rice, J.R., 1993. Estimates from atomic models of tension–shear coupling in dislocation nucleation from a crack tip. Mater. Sci. Eng. A 170, 67–85.

Sunyk, R., Steinmann, P., 2003. On higher gradients in continuum-atomistic modelling. Int. J. Solids Struct. 40, 6877–6896.

Suresh, S., Nieh, T.-G., Choi, B., 1999. Nano-indentation of copper thin films on silicon substrates. Scr. Mater. 41 (9), 951–957.

Tadmor, E.B., Miller, R., Phillips, R., Ortiz, M., 1999. Nanoindentation and incipient plasticity. J. Mater. Res. 14 (6), 2233–2250.

Tadmor, E.B., Miller, R.E., 2007. Quasicontinuum method website. ⟨www.qcmethod.com⟩.

van der Giessen, E., Needleman, A., 1995. Discrete dislocation plasticity: a simple planar model. Modeling Simul. Mater. Sci. Eng. 3, 689–735.

van Vliet, K., Suresh, S., 2002. Simulations of cyclic normal indentation of crystal surfaces using the bubble-raft model. Philos. Mag. A 82 (10), 1993–2001.

van Vliet, K.J., Li, J., Zhu, T., Yip, S., Suresh, S., 2003. Quantifying the early stages of plasticity through nanoscale experiments and simulations. Phys. Rev. B 67, 104105.

Vitek, V., Egami, T., 1987. Atomic level stresses in solids and liquids. Phys. Stat. Solids B 144, 145–156.

Vitek, V., Lejcek, L., Bowen, D.K., 1972. Interatomic Potentials and the Simulation of Defects. Plenum, New York, pp. 493–508.

Voter, A.F., 1997. Hyperdynamics: accelerated molecular dynamics of infrequent events. Phys. Rev. Lett. 78, 3908–3911.

Zhu, T., Li, J., van Vliet, K.J., Ogata, S., Yip, S., Suresha, S., 2004. Predictive modeling of nanoindentation-induced homogeneous dislocation nucleation in copper. J. Mech. Phys. Solids 52, 691–724.

Zienkiewicz, O., Taylor, R., 1989. The Finite Element Method, fourth ed., vol. 1. McGraw-Hill, London.

Zimmerman, J., Kelchner, C., Hamilton, J., Foiles, S., 2001a. Surface step effects on nanoindentation. Phys. Rev. Lett. 87, 165507.

Zimmerman, J., Klein, P.A., Foiles, S.M., 2001b. Effect of surface steps on dislocation structure during nanoindentation. In: Material Research Society Symposium Proceedings, vol. 649, pp. Q8.8.1–Q8.8.6.